6

Wrench Capabilities of Planar Parallel Manipulators and their Effects Under Redundancy

Flavio Firmani[1], Scott B. Nokleby[2], Ronald P. Podhorodeski[1] and Alp Zibil[1]
[1]University of Victoria, [2]University of Ontario Institute of Technology
Canada

1. Introduction

1.1 Instantaneous twist and wrench capabilities

The instantaneous twist and wrench capability analyses are essential for the design and performance evaluation of serial and parallel manipulators. An instantaneous twist is a screw quantity that contains both angular and translational velocities of the end-effector, i.e., $\mathbf{V} = \{\boldsymbol{\omega}^T; \mathbf{v}^T\}^T$. Whereas, a wrench is a screw quantity that contains the forces and moments acting on the end-effector, i.e., $\mathbf{F} = \{\mathbf{f}^T; \mathbf{m}^T\}^T$. For a given pose, the required task of the end-effector is to move with a desired twist and to sustain (or apply) a specific wrench. These kinematic conditions are achieved with corresponding joint velocities $(\dot{\mathbf{q}})$ and joint torques $(\boldsymbol{\tau})$, respectively. The relationship between the task and joint spaces is defined by the well known linear transformations:

$$\dot{\mathbf{x}} = \mathbf{J}\dot{\mathbf{q}} \tag{1}$$

$$\boldsymbol{\tau} = \mathbf{J}^T\mathbf{F} \tag{2}$$

where $\mathbf{J}$ is referred to as the Jacobian matrix.

In addition, an extended problem can be formulated as the analysis of the maximum twist or wrench that the end-effector can perform in the twist or wrench spaces, respectively. The knowledge of maximum twist and wrench capabilities is an important tool for achieving the optimum design of manipulators. For instance, by being able to graphically visualize the twist and wrench capabilities, comparisons between different design parameters, such as the actuator torque capabilities and the dimensions of the links, can be explored. Also, the performance of an existing manipulator can be improved by identifying the optimal capabilities based on the configuration of the branches and the pose of the end-effector.

This work focuses on the wrench capabilities of planar parallel manipulators (PPMs), the geometric interpretation of their wrench polytopes, the derivation of wrench performance indices, and how the inclusion of redundancy affects the performance of parallel manipulators (PMs). The wrench capability analysis of a manipulator depends on its design, posture, and actuator torque capabilities.

Source: Parallel Manipulators, Towards New Applications, Book edited by: Huapeng Wu, ISBN 978-3-902613-40-0, pp. 506, April 2008, I-Tech Education and Publishing, Vienna, Austria

For a 3-degree-of-freedom (DOF) planar manipulator, the wrench $\mathbf{F}$ is a screw quantity that contains the two components of the force on the plane (f_x and f_y) and the moment normal to the plane (m_z). The problem of finding the wrench capabilities of a manipulator involves the forward static force equation ($\mathbf{F} = \mathbf{J}^{-T}\boldsymbol{\tau}$) and the actuator output capabilities (τ_i). To date, three different approaches for determining wrench capabilities have been proposed in the literature: constrained optimization, wrench ellipsoid, and wrench polytope.

1.2 Constrained optimization

In general, the constrained optimization approach involves: an objective function that maximizes either the magnitude of the force f or the moment m_z; one equality constraint ($\mathbf{F} = \mathbf{J}^{-T}\boldsymbol{\tau}$); and a set of inequality constraints ($\tau_{i_{\min}} \le \tau_i \le \tau_{i_{\max}}$), indicating the actuator output capabilities. Kumar and Waldron (1988) investigated force distribution in redundantly-actuated closed-loop kinematic chains and concluded that there would be zero internal forces using the Moore-Penrose pseudo-inverse solution. Tao and Luh (1989) developed an algorithm that determines the minimum torque required to sustain a common load between two joint redundant cooperating manipulators. Nahon and Angeles (1992) described the problem of a hand grasping an object as a redundantly-actuated kinematic chain. The problem was formulated with both equality and inequality constraints and the torques were found by minimizing the internal forces in the system using Quadratic Programming. Buttolo and Hannaford (1995) analyzed the force capabilities of a redundant planar parallel manipulator. Torques were optimized using the ∞-norm resulting in higher force capabilities when compared to the pseudo-inverse solution. Nokleby et al. (2005) developed a methodology to optimize the force capabilities of redundantly-actuated planar parallel manipulators using an n-norm, for large values of n, and a scaling factor. Garg et al. (2007) implemented this approach to spatial parallel manipulators.
This approach is usually slow due to the numerical nature of the algorithm and inaccuracies due to the existence of local minima.

1.3 Wrench ellipsoid

The wrench ellipsoid approach is based on bounding the actuator torque vector by a unit sphere $\boldsymbol{\tau}^T\boldsymbol{\tau} \le 1$. The torques are mapped into the wrench space with Eq.(2), yielding a force ellipsoid $\mathbf{F}^T\mathbf{J}\mathbf{J}^T\mathbf{F} \le 1$. If Singular Value Decomposition (SVD) is applied to $\mathbf{J}$ i.e., $\mathbf{J} = \mathbf{U}\Sigma\mathbf{V}^T$, the principal axes of the ellipsoid can be determined as $\mathbf{u}_k / \sigma_k$ where σ_k is the k^{th} singular value and $\mathbf{u}_k$ is the k^{th} column of matrix $\mathbf{U}$. These axes can be employed as wrench performance indices of the manipulator. This approach was introduced by Yoshikawa (1985) with the manipulability (twist) ellipsoid and proposed manipulability measurements. Also, Yoshikawa (1990) presented the duality between the twist and wrench ellipsoids concluding that axes of the ellipsoids coincide but their lengths are inversely proportional.
For cooperating manipulators, Chiacchio et al. (1996) presented a complete analysis of wrench ellipsoids for multiple-arm systems, which involves external and internal forces. Lee and Kim (1991) (velocity problem) and Chiacchio et al. (1997) (static force problem) proposed to normalize the joint space variables (joint velocities and joint torques, respectively) when the actuators do not produce the same output. As a result, the resulting ellipsoid is defined as the pre-image of the unit sphere in the scaled joint variable space.

The wrench ellipsoid approach can be implemented easily and the required computation is immediate. However, this approach is an approximation because the joint torques are normalized ($\boldsymbol{\tau}^{\mathrm{T}}\boldsymbol{\tau} \leq 1$) yielding a hypersphere in the torque space. The correct model of the joint torques must be an m-dimensional parallelepiped in the torque space due to the nature of the extreme torque capabilities of each actuator, i.e., $\tau_{i_{\min}}$ or $\tau_{i_{\max}}$.

1.4 Wrench polytope

The wrench polytope approach considers the complete region in which the actuator can operate. A comparison between the ellipsoid approach and the polytope approach is shown in Fig. 1. Assume a manipulator with two actuated revolute joints whose extreme capabilities are $\tau_{i_{\text{ext}}} = \pm 1$ Nm, for i = 1, 2. Fig. 1a shows the generation of an ellipse (in general, an ellipsoid) as a result of mapping a circle (in general, a hypersphere). Fig. 1b shows the generation of a polygon (in general, a polytope) as a result of mapping a square (in general, a hypercube). Each plot contains two coordinate systems. The inner circle of Fig. 1a and the inner square of Fig. 1b describe the torque limits in the torque space (bottom and left axes); whereas, the outer ellipse and polygon describe the wrench capabilities in the wrench space (top and right axes). The lines that connect the inner to the outer shapes illustrate the linear transformation. Note how the edges and vertices of the square and polygon correspond in both spaces. The areas comprised by these geometrical shapes represent the feasible capabilities in their corresponding spaces. The square is an exact representation of the torque capabilities; while, the circle is an approximation. For example, the upper-right vertex of the square is $\tau_1 = \tau_2 = 1$ Nm; although this torque combination is feasible, the circle model does not include it. Thus, modeling the torque capabilities as a square is better than as a circle. Fig. 1c shows how the circle and ellipse are inscribed within the square and polygon, respectively. It is important to mention that the principal axes of the ellipse are directed towards the vertices of the polygon.

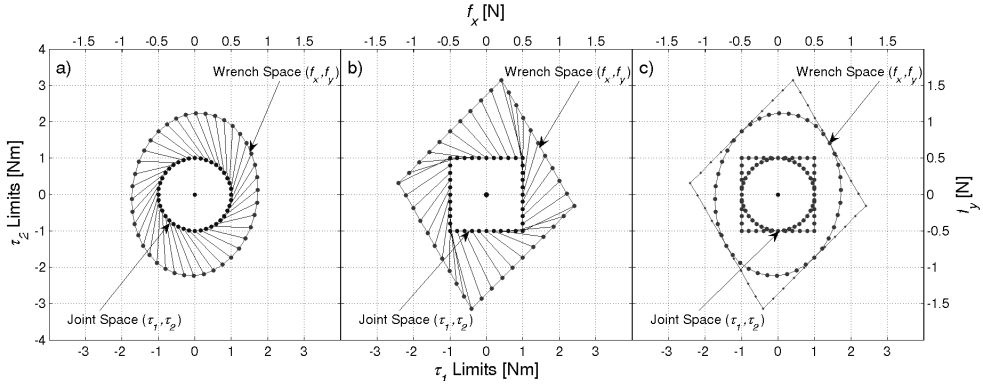

Fig. 1. Mapping of ellipsoids and polytopes from the joint space to the task space.

In general, each actuator torque defines an orthonormal axis in $\mathbb{R}^m$. The extremes of each torque constrain the torque space with a pair of parallel planes along each axis. The feasible region in which the manipulator can operate is bounded by these pairs of parallel planes yielding an *m*-dimensional parallelepiped.

A linear transformation, such as the equation of the forward static force, Eq. (2), maps vector $\boldsymbol{\tau}$ from $\mathbb{R}^m$ (joint torque space) to $\mathbb{R}^n$ (wrench space).
Rockafellar (1997) studied the properties of convex polyhedral sets. From his analysis, the following relationship is held through a linear transformation: Let $\boldsymbol{\tau}$ be the *m*-dimensional parallelepiped (a convex set) and $\mathbf{J}^{-T}$ be the linear transformation from $\mathbb{R}^m$ to $\mathbb{R}^n$. Then the resulting transformation $\mathbf{J}^{-T}\boldsymbol{\tau}$ leads to another convex polyhedral set ($\mathbf{F}$) in $\mathbb{R}^n$ and it contains a finite number of facets.
Kokkinis and Paden (1989) introduced the concept of twist and wrench convex polytopes. The analysis was applied to a single serial manipulator and to two cooperating manipulators. Chiacchio et al. (1997) analyzed the wrench polytopes of redundant serial manipulators. Finotello et al. (1998) introduced two sets of indices that can be implemented to twist and wrench polytopes: the maximum isotropic value (MIV) and the maximum available value (MAV). These indices will be discussed in detail in Section 4. For 6-DOF manipulators, Finotello et al. (1998) proposed to analyze these indices with force and moment as separate entities. Gallina et al. (2001) analyzed the manipulability of a 3-DOF wire driven planar haptic device using polytopes. Lee and Shim (2004) expanded the concept to dynamic manipulability of multiple cooperating manipulators resulting in acceleration polytopes. Krut et al. (2004a) analyzed twist ellipsoids and polytopes in redundant parallel manipulators and established performance indices. They showed that there is another ellipsoid, besides the one derived with SVD, which is larger in volume and is fully inscribed within the polytope. Krut et al. (2004b) also studied force performance indices of redundant parallel manipulators and determined the isotropic wrench workspaces of planar wire-driven manipulators with multiple actuated limbs. Firmani et al. (2007a and 2007b) derived a set of wrench performance indices for PPMs.

2. Redundancy

2.1 Types of redundancy

Merlet (1996) described that the inclusion of redundancy may lead to improvements in various analyses such as forward kinematics, singular configurations, optimal force control, and calibration. Lee and Kim (1993) defined a redundant parallel manipulator as one that has an infinite number of choices for either generating motion or resisting external forces. Also, Lee and Kim (1993) presented an analysis of different types of redundancy. Ebrahimi et al. (2007) classified redundancy into two categories: kinematic and actuation redundancy.

2.2 Kinematic redundancy

A manipulator is termed kinematically redundant when at least one of the branches can have self-motion while keeping the mobile platform fixed. Thus, there is an infinite number of possible solutions to the inverse displacement problem. This is the typical case of redundant serial manipulators. For parallel manipulators, this redundancy happens when the number of joints of at least one branch is greater than the number of joints that are required to provide the desired mobility of the mobile platform. This type of redundancy allows self-motion of the redundantly-jointed branch(es) improving the dexterity and workspace of the manipulator. A draw back of this type of redundancy is the increase of mass and/or inertia due to the addition of actuators on the mobile links. Despite the redundancy, there is only one vector force per branch acting on the mobile platform. Thus,

the load capability cannot be optimized, but as an alternative, the direction of the branch forces can be optimized by changing the posture of the redundantly-jointed branch(es). With this type of redundancy, each actuator can be manipulated independently and there are no internal forces that could damage the device. Kinematic redundancy can be employed to reduce or even eliminate singular configurations. Wang and Gosselin (2004) added an extra revolute joint to one branch of the 3-RPR PPM yielding a RRPR-2RPR layout. The singularity conditions were identified and the singularity loci were reduced. Ebrahimi et al. (2007) proposed the 3-PRRR PPM, a layout that contains joint redundancy in every branch. This manipulator can provide singularity free paths and obstacle avoidance by properly manipulating the actuated joints.

2.3 Actuation redundancy

A parallel manipulator is termed redundantly actuated when an infinite number of resultant force combinations can span the system of external forces. Thus, there is an infinite number of solutions to the inverse static force problem. The implementation of this redundancy requires a reliable control system because a small variation in the displacement may cause severe damage to the manipulator. There are two types of actuation redundancy: in-branch redundancy and branch redundancy.

In-Branch Redundancy. Passive joints are replaced by active joints. For every redundant actuator added within branch(es), the number of the forces resisting an external load is augmented by one. This type of redundancy can be easily incorporated into an existing device. Nokleby et al. (2005) developed a methodology to optimize the force capabilities of the 3-RRR PPM using a high norm and a scaling factor. Zibil et al. (2007) determined the force capabilities of the 3-RRR PPM by using an analytical based method. Nokleby et al. (2007a) investigated the force-moment capabilities of different in-branch redundancy architectures. With in-branch redundancy, there is no change in the workspace of the manipulator. However, there is an increase of mass and/or inertia due to the addition of actuators. Firmani & Podhorodeski (2004) eliminated families of singular configurations by adding a redundant actuator to the 3-RRR PPM, yielding a RRR-2RRR layout.

Branch Redundancy. An additional actuated branch is added to the system. For every additional actuated branch incorporated into the system, the number of forces acting on the mobile platform is augmented by one. Buttolo and Hannaford (1995) designed and analyzed the force capabilities of a 2-DOF 3-RRR PPM haptic device, where all three branches are pinned together. Gallina et al. (2001) analyzed the maximum force and moment of a four-wire driven 3-DOF planar haptic device. Krut et al. (2004a) implemented performance indices, previously developed in Krut et al. (2004b) for velocity analysis, to 2-DOF parallel wire-driven manipulators. Different analyses of multi-actuated wires were considered. Nokleby et al. (2007b) investigated the force-moment capabilities of the 4-RRR, 4-RPR, and 4-PRR PPMs. Firmani & Podhorodeski (2005) presented a methodology to identify singular configurations of planar parallel manipulators with redundant branches. The main problem of manipulators with branch redundancy is the reduction of their dexterity and workspace.

3. Wrench polytope analysis

3.1 Joint space parallelepiped

Let n be the DOF of the task space coordinates and m be the number of actuated joints. The i^{th} joint torque variable, which is bounded by $\tau_{i_{\min}}$ and $\tau_{i_{\max}}$, can be represented in the joint

torque space as two parallel planes in $\mathbb{R}^m$. With *m* joints, there are *2m* planes or *m* pairs of parallel planes. An *m*-dimensional parallelepiped is formed with the combination of all of these parallel planes yielding the region of joint torque capabilities. If all the torque capabilities were equal, the *m*-dimensional parallelepiped would result in a hypercube. Also, if the magnitude of the extreme torques were equal, i.e., $\left|\tau_{i_{\min}}\right| = \left|\tau_{i_{\max}}\right|$, the parallelepiped would be centro-symmetric; otherwise it would be skewed.
A vertex of the *m*-dimensional parallelepiped defines the intersection of *m* extreme torque planes. Thus, a vertex occurs when all joint torques are at their extreme capabilities, i.e.,

$$v_j = \begin{bmatrix} \tau_{1_{\text{ext}}} & \tau_{2_{\text{ext}}} & \dots & \tau_{m_{\text{ext}}} \end{bmatrix}^{\mathrm{T}} \tag{3}$$

where $\tau_{i_{\text{ext}}}$ denotes the extreme capabilities of the i^{th} actuator, i.e., $\tau_{i_{\min}}$ or $\tau_{i_{\max}}$. The total number of vertices in the *m*-dimensional parallelepiped is $v_{T_m} = 2^m$ (Chiacchio et al., 1997).

3.2 Linear transformation

Visvanathan and Milor (1986) investigated the problems in analog integrated circuits while accounting for the tolerance variations of the principal process parameters. The problem involved the mapping of a parallelepiped under a linear transformation. Their mathematical formulation is similar to the one used for analyzing wrench capabilities in this work. Let the coordinates of the vertices of a parallelepiped in $\mathbb{R}^m$ be v_j, for j = 1, ..., 2^m. Through a linear transformation from $\mathbb{R}^m$ to $\mathbb{R}^n$, such as $\mathbf{F} = \mathbf{J}^{-\mathrm{T}}\boldsymbol{\tau}$, the *m*-dimensional parallelepiped becomes a polytope (Visvanathan and Milor, 1986). A polytope is a convex region, i.e., any two points inside the polytope can be connected by a line that completely fits inside the polytope. An *n*-dimensional convex polytope is bounded by (*n-1*)-dimensional facets or hyperplanes, e.g., linear edges in $\mathbb{R}^2$ bounding a polygon or planar facets in $\mathbb{R}^3$ bounding a polyhedron.
A polytope $\boldsymbol{P}$ can be completely characterized by mapping all the vertices of the parallelepiped and enclosing them in a convex hull, i.e.,

$$\boldsymbol{P} = \text{convh}\left\{ \mathbf{J}^{-\mathrm{T}} v_j , j = 1,\dots,2^m \right\} \tag{4}$$

where convh denotes a convex hull operator which encloses all the extreme points forming the feasible region of the torque space in the wrench space. A closed bounded convex set is the convex hull of its extreme points (Rockefellar, 1997).
The total number of vertices in the polytope (v_{T_n}) depends on the dimension of the two spaces.

3.3 Non-redundant planar manipulators

For non-redundant manipulators (*n* = *m*) the number of vertices in the polytope equals the number of vertices in the *m*-dimensional parallelepiped, i.e., $v_{T_n} = v_{T_m} = 2^m$, and the vertices

of the polytope are the image of the vertices of the *m*-dimensional parallelepiped (Chiacchio et al., 1996), i.e.,

$$p_j = \mathbf{J}^{-\mathrm{T}} v_j \tag{5}$$

where p_j and v_j are the vertices of the polytope and parallelepiped, respectively.

The linear transformation between the two spaces also makes that the edges and facets of the polytope are the corresponding image of the edges and facets of the *m*-dimensional parallelepiped.

For a planar parallel manipulator the vertices of the wrench polytope are found as follows:

$$\begin{aligned} p_j &= \mathbf{J}^{-\mathrm{T}} v_j \\ \begin{bmatrix} f_x \\ f_y \\ m_z \end{bmatrix} &= \begin{bmatrix} \gamma_{1,1} & \gamma_{1,2} & \gamma_{1,3} \\ \gamma_{2,1} & \gamma_{2,2} & \gamma_{2,3} \\ \gamma_{3,1} & \gamma_{3,2} & \gamma_{3,3} \end{bmatrix} \begin{bmatrix} \tau_{1_{\mathrm{ext}}} \\ \tau_{2_{\mathrm{ext}}} \\ \tau_{3_{\mathrm{ext}}} \end{bmatrix} \end{aligned} \tag{6}$$

where $\gamma_{i,j}$ denotes the elements of $\mathbf{J}^{-\mathrm{T}}$. There are eight vertices (2^3) due to the combination of the extreme torque capabilities, i.e., $\tau_{i_{\mathrm{ext}}}$ can be either $\tau_{i_{\mathrm{min}}}$ or $\tau_{i_{\mathrm{max}}}$.

Fig. 2 illustrates the linear transformation of the torque capabilities of a non-redundant planar parallel manipulator from the torque space to the wrench space. Fig. 2 also shows the corresponding image of the vertices, edges, and facets between the parallelepiped and the polytope.

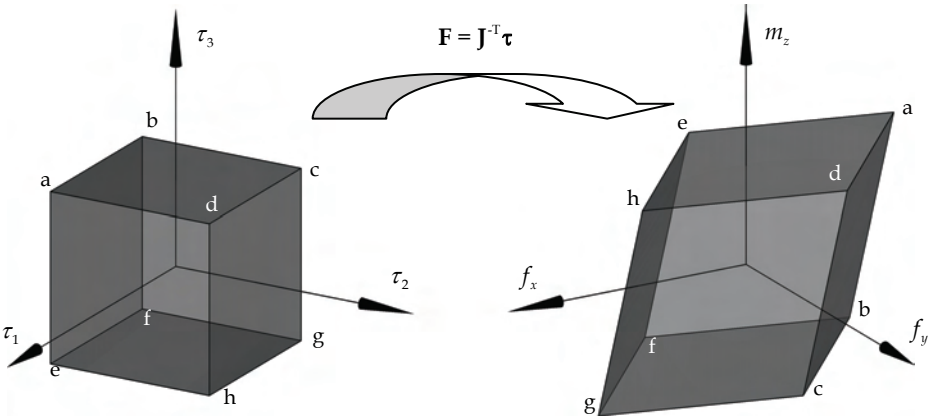

Fig. 2. Linear transformation of a parallelepiped to a polytope of a non-redundant PPM and image projection of vertices, edges, and facets.

The resulting wrench polytope of a non-redundant manipulator has the following characteristics:

i. Any point outside the polytope is a wrench that cannot be applied or sustained;
ii. Any point inside the polytope is achieved with actuators that are not working at their extreme capabilities;

iii. Any point on a facet of the polytope has one actuator working at an extreme capability;
iv. Any point on an edge of the polytope has two actuators working at their extremes;
v. Any vertex of the polytope has all three actuators working at their extremes.

3.4 Redundant manipulators

For redundant manipulators ($n < m$) the number of vertices in the polytope is less than the vertices of the m-dimensional parallelepiped, i.e., $v_{T_n} < v_{T_m}$. In this case, the vertices of the polytope are formed with the mapping of some of the vertices of the m-dimensional parallelepiped, i.e.,

$$p_k \subset \mathbf{J}^{-\mathrm{T}} v_j \tag{7}$$

with $k < j$. The points that do not form the vertices of the polytope are internal points in $\boldsymbol{P}$.
Let the potential vertices (p_j) of the polytope be all the projected vertices of the m-dimensional parallelepiped in $\mathbb{R}^n$. Thus, the potential vertices are determined as follows:

$$\begin{aligned} p_j &= \mathbf{J}^{-\mathrm{T}} v_j \\ \begin{bmatrix} f_x \\ f_y \\ m_z \end{bmatrix} &= \begin{bmatrix} \gamma_{1,1} & \gamma_{1,2} & \cdots & \gamma_{1,m} \\ \gamma_{2,1} & \gamma_{2,2} & \cdots & \gamma_{2,m} \\ \gamma_{3,1} & \gamma_{3,2} & \cdots & \gamma_{3,m} \end{bmatrix} \begin{bmatrix} \tau_{1_{\mathrm{ext}}} \\ \tau_{2_{\mathrm{ext}}} \\ \vdots \\ \tau_{m_{\mathrm{ext}}} \end{bmatrix} \end{aligned} \tag{8}$$

The number of external vertices may vary. For instance, the projection of a cube on a plane may lead to six external vertices (general projection) or four external vertices (projection normal to a coordinate axis).
The number of vertices of the wrench polytope depends on the pose of the manipulator, which defines the elements of the linear transformation matrix, $\mathbf{J}^{-\mathrm{T}}$.
Finding the external vertices of a polytope can be computationally expensive. Generating a polytope through a convex hull has been studied thoroughly in the field of computational geometry and the goal has been to make a more efficient algorithm. Chand and Kapur (1970) proposed the so-called gift wrapping algorithm, where the facets of a polytope are found by determining the angles between one vertex and the rest of the points. The minimum and maximum angles correspond to the hyperplanes passing through that point. Visvanathan and Milor (1986) proposed an algorithm that searches in the directions that are orthogonal to each of the known hyperplanes. New vertices and hyperplanes are formed and the process is repeated. Bicchi et al. (1995) presented an algorithm that involves slack variables that transform the inequality constraints of the actuator limits into equality constraints. Lee (1997) proposed a method for determining the vertices of twist polytopes using vector algebra. Hwang et al. (2000) developed a recursive algorithm that removes all the internal points when first encountered. Hwang et al. (2000) also showed that even though the number of potential vertices grows exponentially (2^m), the number of external points increases linearly.

The scope of this work is not to develop a new algorithm for determining the external vertices and facets of a polytope, although some of the concepts that will be described in this work may be used to generate an even more efficient algorithm.

The geometrical interpretation of the internal points is illustrated with the following example. Assume a planar manipulator with a redundant joint. Thus, the linear transformation maps the torque capabilities from $\mathbb{R}^4$ to $\mathbb{R}^3$.

Fig. 3 illustrates the resulting polytope as a wire frame. This polytope is formed with the convex hull of the extreme points. The same polytope is repeated in all the sub-plots. Each sub-plot shows the regions in which one of the actuator torques is working at its extreme capabilities. The darker and lighter regions denote the two extremes $\tau_{i_{\min}}$ and $\tau_{i_{\max}}$, respectively. These regions are convex sets themselves, here defined as inner polytopes. The un-shaded region of each plot represents the space in which the actuator works within its capabilities.

The overall polytope was generated with 16 potential vertices, of which 14 are external and 2 are internal. The external vertices are illustrated with dots. Internal vertices lead to particularly low wrenches despite having all toques working at their extreme capabilities.

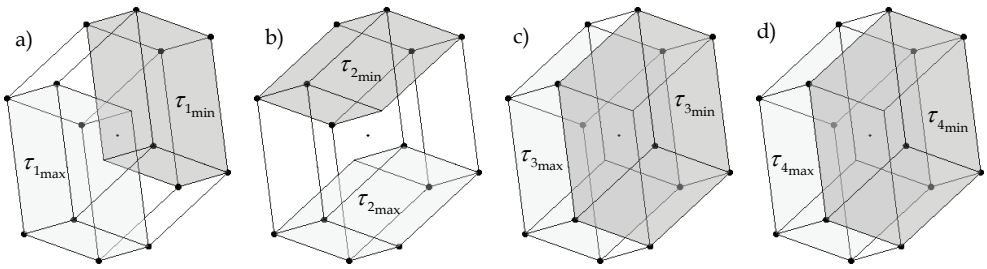

Fig. 3. Polytope of a redundant planar parallel manipulator with shaded regions showing torques at extreme capabilities: a) Extremes of τ_1, b) Extremes of τ_2, c) Extremes of τ_3, and d) Extremes of τ_4.

Based on these plots, the following conclusions can be made. While for a non-redundant manipulator each facet of the *m*-dimensional parallelepiped corresponded to a facet of the polytope; for a redundant manipulator this projection leads to volumes in the polytope. Also, each edge of the polytope is defined with the projection of three torques set at their extremes; while, each facet is formed with two torques at their extremes.

Further actuation would result in more complicated polytopes and the number of internal points will increase exponentially (Hwang et al., 2000). In general, the number of geometrical entities in a wrench polytope is determined with the number of combinations involving torque at their extreme capabilities and the associated magnitude, e.g., say $\tau_{i_{ext}}$ is at an extreme capability which can be of magnitude $\tau_{i_{\min}}$ or $\tau_{i_{\max}}$. The number of geometrical entities is summarized in Table 1.

Geometrical Entity (Internal and External)	Actuators at Extreme	Number of Geometrical Entities
Vertices	m	2^m
Edges	m-1	$2^{m-1}m$
Facets	m-2	$2^{m-3}(m-1)m$

Table 1. Geometrical entities of a wrench polytope for redundant manipulators.

The resulting wrench polytope of a redundant manipulator has the following characteristics:

i. Any point outside the polytope is a wrench that cannot be applied or sustained;
ii. Any point inside the polytope is achieved with actuators that may or may not work at their extreme capabilities;
iii. Any point on a facet of the polytope has m-2 actuators working at their extremes;
iv. Any point on an edge of the polytope has m-1 actuators working at their extremes;
v. Any vertex of the polytope has all m actuators working at their extremes.

4. Wrench performance indices

4.1 Operational conditions

A wrench polytope represents the region in which the manipulator can apply feasible wrenches. Unfortunately, a major drawback of this approach compared to the ellipsoid approach is the efficiency of the algorithm. Determining the axes of the ellipsoid by applying SVD to $\mathbf{J}$ is definitely more efficient than constructing a polytope. A small eigenvalue indicates that the manipulator requires large actuator torques to sustain an exerted wrench.

Nonetheless, the best representation, from a design perspective, may not be the polytope itself, but rather a set of indices that characterize it. These points may lie on facets, edges, or vertices of the wrench polytope, and represent maximum/minimum values of either moments or forces. Thus, these points, which are referred to as wrench performance indices, allow the determination of either force or moment ranges.

Under operational conditions, the manipulator performance is dictated by the requirements of the application. These requirements establish some parameters of moments and forces acting on the manipulator. This is, the range of forces can be determined based on moment requirements; similarly, the range of moments can be determined based on force requirements. For the force analysis, there are two ranges of forces that can be determined. Finotello et al. (1998) defined these forces as maximum available value (MAV) and maximum isotropic value (MIV). Herein, MAV and MIV are denoted as F_{av} and F_{is}, respectively.

Assume a wrench with a constant moment, thus the polytope is reduced to a polygon, i.e., the polytope is sliced at the constant moment yielding a polygon. The area enclosed by the polygon represents the force capabilities of the manipulator. The maximum available force (F_{av}) is the farthest distance from the center of the force space to the polygon. This force can be only applied in a particular direction and corresponds to a vertex of the polygon. The maximum isotropic force (F_{is}) is the shortest distance from the center of the force space to the polygon. Fig. 4 illustrates the force polygon of a 3-RRR PPM, where the underline denotes the actuated joints and is indicated in the figure with τ_1, τ_2, and τ_3. For an arbitrary

direction α, the distance from the center of the force space to any point within the polygon is proportional to the magnitude of the force that can be applied or sustained. Fig. 4 also shows an arbitrary force vector $\mathbf{f} = [f_x, f_y]^T = [f\cos\alpha, f\sin\alpha]^T$ and the maximum available (F_{av}) and isotropic (F_{is}) forces.

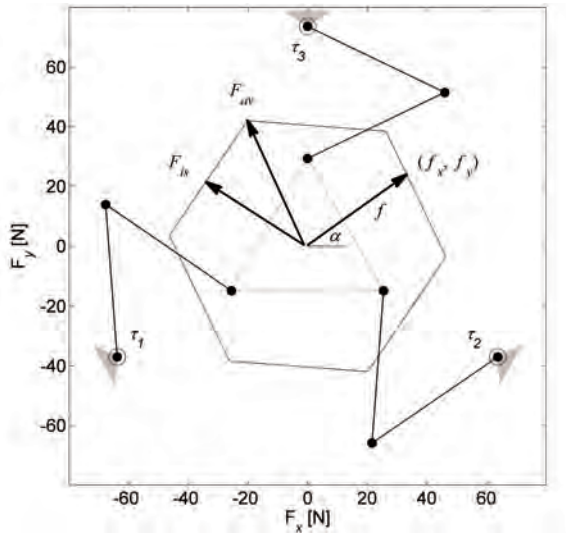

Fig. 4. Force polygon and force capabilities.

In this work, six different scenarios of operational conditions in which the forces and moments interact are presented. Table summarizes the six operational conditions which lead to two force analyses and four moment analyses.

Operational Condition	Analysis
Prescribed Moment	Force Analysis: Find Range of Available and Isotropic Forces
Largest Allowable Force with an Associated Moment	
Prescribed Force (magnitude and direction)	Moment Analysis: Find Range of Moments
Largest Allowable Moment with an Associated Force	
Prescribed Isotropic Force (magnitude)	
Prescribed Available Force (magnitude)	

Table 2. Operational condition and corresponding analyses.

4.2 Explicit analysis

To determine a particular performance index, Eq. (8) is rearranged as a linear system of three equations of the form **Ax** = **b**; where **x** is a vector that contains all of the unknown variables, either wrench or torque space coordinates, **A** is a coefficient matrix, and **b** is a vector that contains the torques that are set to their extreme capabilities.

If the performance index value lies on a vertex of the polytope, all *m* actuators will be set to their extreme capabilities. There are 2^m possible combinations due to the two extreme magnitudes of the torque outputs ($\tau_{i_{\min}}$ or $\tau_{i_{\max}}$).

If the performance index value lies on an edge of the polytope, *m-1* actuators are set to their extreme output capabilities, while the remaining actuator torque is working within its output range and is referred to as being in transition (τ_t). Torques that are not at their extreme capabilities are said to be in transition because they transfer from one torque limit to the opposite limit, e.g., from $\tau_{i_{\min}}$ to $\tau_{i_{\max}}$. A torque in transition is an unknown variable in vector **x**. There are $2^{m-1}m$ combinations.

If the performance index value lies on a facet of the polytope, *m-2* actuators are set to their extreme capabilities and two torques are in transition. There are $2^{m-3}(m-1)m$ combinations.

Once all the combinations are evaluated, the performance index can be determined by verifying the maximum *f* or m_z among all of the combinations. If the problem involves finding a torque in transition, it is important to verify that this torque does not exceed its torque output capabilities.

Table 3 summarizes the operational condition, the number of actuators working at their extreme capabilities, a list of known and unknown variables, and the number of combinations that are required to evaluate. This procedure is equivalent for both non-redundant and redundant planar parallel manipulators.

Operational Condition	Actuators at Extremes	Variables Known | Unknown	Number of Combinations
Maximum Force with a Prescribed Moment ($^{\text{pm}}F_{av}$ and $^{\text{pm}}F_{is}$)	*m - 1*	$m_z \mid f_x$ and f_y	$2^{m-1}m$
Maximum Allowable Force with an Associated Moment ($^{\text{am}}F_{av}$ and $^{\text{am}}F_{is}$)	*m*	$\mid m_z, f_x$ and f_y	2^m
Maximum Moment with a Prescribed Force ($^{\text{pf}}M_z$)	*m - 2*	f_x and $f_y \mid m_z$	$2^{m-3}(m-1)m$
Maximum Allowable Moment with an Associated Force ($^{\text{af}}M_z$)	*m*	$\mid m_z, f_x$ and f_y	1
Maximum Moment with a Prescribed Isotropic Force ($^{\text{pif}}M_z$)	*m - 2*	$f \mid m_z$ and α	$2^{m-3}(m-1)m$
Maximum Moment with a Prescribed Available Force ($^{\text{paf}}M_z$)	*m* *m – 1*	$\mid m_z, f_x$ and f_y $f \mid m_z$ and α	2^m $2^{m-1}m$

Table 3. Wrench performance indices of planar parallel manipulators.

4.2 Force analysis

Maximum Force with a Prescribed Moment. If the moment must be preserved in the requirements of the application, either zero or any other value, the polytope is reduced to a polygon. In Fig 5a, the dark area illustrates the polygon at $m_z=0$, while the other lines show

polygons at different moments. For this problem, m_z must be specified yielding the following set of unknown variables: $\mathbf{x} = [f_x \quad f_y \quad \tau_t]^{\mathrm{T}}$. Thus, Eq. (8) is rearranged as follows:

$$\mathbf{Ax} = \mathbf{b}$$

$$\begin{bmatrix} 1 & 0 & -\gamma_{1,t} \\ 0 & 1 & -\gamma_{2,t} \\ 0 & 0 & -\gamma_{3,t} \end{bmatrix} \begin{bmatrix} f_x \\ f_y \\ \tau_{\mathrm{t}} \end{bmatrix} = \begin{bmatrix} \gamma_{1,1} & \cdots & \gamma_{1,t-1} & \gamma_{1,t+1} & \cdots & \gamma_{1,m} \\ \gamma_{2,1} & \cdots & \gamma_{2,t-1} & \gamma_{2,t+1} & \cdots & \gamma_{2,m} \\ \gamma_{3,1} & \cdots & \gamma_{3,t-1} & \gamma_{3,t+1} & \cdots & \gamma_{3,m} \end{bmatrix} \begin{bmatrix} \tau_{1_{\mathrm{ext}}} \\ \vdots \\ \tau_{t-1_{\mathrm{ext}}} \\ \tau_{t+1_{\mathrm{ext}}} \\ \vdots \\ \tau_{m_{\mathrm{ext}}} \end{bmatrix} - \begin{bmatrix} 0 \\ 0 \\ m_z \end{bmatrix} \tag{9}$$

The maximum available force $({}^{\mathrm{pm}}F_{av})$ corresponds to the largest value of f that is evaluated with the combinations, where $f = \sqrt{f_x^{\,2} + f_y^{\,2}}$. The maximum isotropic force $({}^{\mathrm{pm}}F_{is})$ is determined as the shortest distance from the center of the force space to the polygon. ${}^{\mathrm{pm}}F_{av}$ and ${}^{\mathrm{pm}}F_{is}$ represent a point on an edge and a point on a facet of the polytope.

Maximum Allowable Force with an Associated Moment. If a moment does not affect the requirement of the application, the manipulator can reach the largest available and isotropic forces. To achieve these forces a particular moment must be associated with them. The set of unknown variables of the **Ax = b** problem is $\mathbf{x} = [f_x \quad f_y \quad m_z]^{\mathrm{T}}$. A force polygon may be generated by projecting the vertices of the polytope on the force plane. Fig 5 b illustrates the projection of the polytope vertices on the force space plane. The available and isotropic forces $({}^{\mathrm{am}}F_{av}$ and ${}^{\mathrm{am}}F_{is})$ are respectively the longest and shortest distances from the center of the force space to the projected polygon.

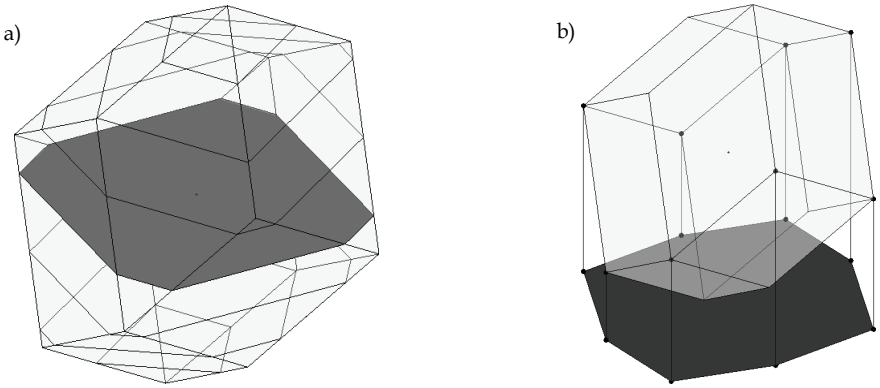

Fig. 5. Force analysis: a) Maximum force with a prescribed moment and b) Maximum force with an associated moment.

4.3 Moment analysis

Maximum Moment with a Prescribed Force. For a fully described force (f and α), the force vector may be drawn within the polytope and the set of moments $({}^{\mathrm{pf}}M_z)$ that can be reached with this force can be determined. Eq. (8) is rearranged as an **Ax = b** problem with

$\mathbf{x} = [m_z \quad \tau_{t_a} \quad \tau_{t_b}]^T$. The largest and smallest m_z that can be obtained while keeping the torques in transition within their capabilities define the range of ${}^{\text{pf}}M_z$. Fig. 6a illustrates an arbitrary force and the vertical line represents the range of moments.

Maximum Allowable Moment with an Associated Force. If the force does not affect the application, the maximum range of moments $({}^{\text{af}}M_z)$ has an associated force, i.e., a specific force must be applied to achieve the largest moment. To find the maximum moment all the actuators are set to their maximum capabilities. To achieve the largest range of ${}^{\text{af}}M_z$, the third row of Eq. (8) is arranged to obtain the combination of monomials that yields the maximum and the minimum m_z. Thus, only a single evaluation is required for each extreme value. The highest and lowest vertices of the polytope represent this performance index.

Maximum Moment with a Prescribed Isotropic Force. Assume that the manipulator is required to apply or sustain the same force in all directions, i.e., an isotropic force f_{is}. The region of moments that can attain this force may be seen as a cylinder of radius f_{is} that is fully contained within the polytope, as shown in Fig. 6b. The range of moments $({}^{\text{pif}}M_z)$ is the height of the cylinder. The cylinder intersects facets of the polytope. This case cannot be solved by simply rearranging Eq. (8). As an alternative, the maximum and minimum ${}^{\text{pif}}M_z$ are determined by comparing the resulting isotropic moment associated with every plane of the polytope. Isotropy is ensured with the plane that yields the minimum of the maximum m_z moment. A detailed formulation of this problem is described in Firmani et al. (2007a).

Maximum Moment with a Prescribed Available Force. Assume that the manipulator is required to apply a large force regardless of its direction, i.e., available force f_{av}. This case may be seen as the intersection of a cylinder of radius f_{av} with a point on the polytope which is the farthest away from the m_z=*0* plane, as shown in Fig 6c. The range of moments $({}^{\text{paf}}M_z)$ is the height of this cylinder. The cylinder usually intersects an edge of the polytope, but in some particular cases the intersection may happen with a facet of a vertex of the polytope.

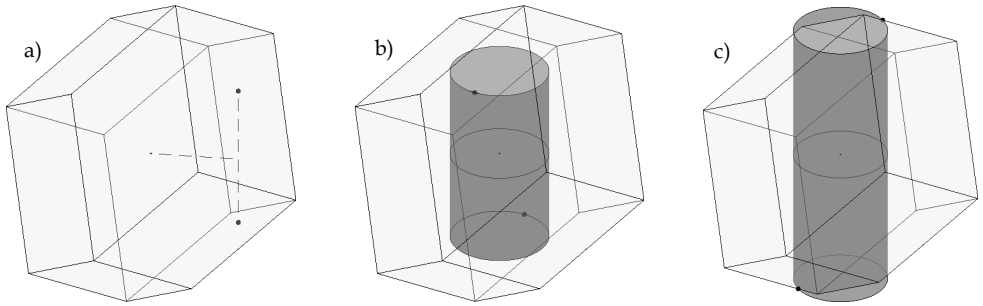

Fig. 6 Moment analysis. Maximum moment with a prescribed a) Force, b) Isotropic force, and c) Available force.

5. Wrench workspaces

5.1 Planar parallel manipulator architectures

For three-branch PPM layouts, there are seven possible architectures: RRR, RPR, PRR, RRP, PPR, RPP, and PRP, where R and P denote a revolute and prismatic joint, respectively. Of these seven architectures, the PRR and the RRP are kinematically equivalent. Likewise, the

PPR and the RPP. Considering only one kinematically equivalent architecture yields only five unique architectures. Eliminating those architectures with two prismatic joints, as they are not convenient for implementation as PPMs, leaves only the RRR, RPR, and PRR architectures to be studied. Based on these architectures, three actuation schemes are analyzed: non-redundant PPMs, in-branch redundant PPMs, and branch redundant PPMs.

Non-Redundant PPMs. By considering the first joints actuated, the inertia of the mechanism is kept low allowing manipulators to be used for high-speed applications. Thus, the actuation layouts 3-RRR, 3-RPR, and 3-PRR are considered. Fig. 7 shows the schematics of the three non-redundant PPM layouts. The fixed and mobile platforms are similar in every case: the base triangle edge lengths are 0.5 m and the end-effector triangle edge lengths are 0.2 m. For the 3-RRR, the lengths of the first and second links of each branch are 0.2 m. The torque limits of the actuators are ±4.2 Nm. For the 3-RPR, the torque limits are ±4.2 Nm and the prismatic joints' extension limits are 0.0 to 0.4 m. For the 3-PRR, the prismatic joints' orientations are 0°, 120°, 240°, the prismatic joints' extension limits are 0.0 to 1.0 m and the force limits are ±10 N, while the lengths of the second links are 0.23 m.

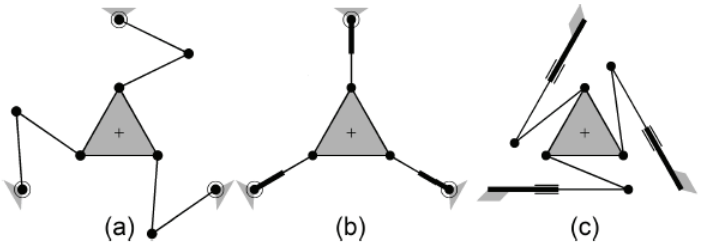

Fig. 7. Non-redundant PPM layouts: a) 3-RRR, b) 3-RPR, c) 3-PRR

In-Branch Redundant PPMs. With this actuation scheme, the second joints of every branch are actuated yielding the 3-RRR, 3-RPR, and 3-PRR layouts. Fig. 8 shows schematics of the in-branch redundant PPM layouts. These PPMs have the same dimensions and actuator capabilities as the ones used for the non-redundant PPMs. In addition, for the 3-RRR and the 3-PRR the second joint is actuated and the torque limits are ±2.1 Nm; whereas, for the 3-RPR, the force limits of the prismatic joints are ±10 N.

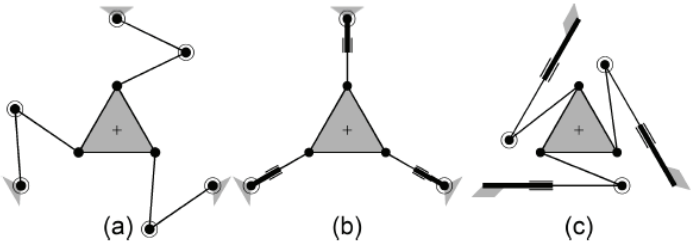

Fig. 8. In-branch redundant PPM layouts: a) 3-RRR, b) 3-RPR, c) 3-PRR

Branch Redundant PPMs. An additional branch is added to the non-redundant PPMs yielding the 4-RRR, 4-RPR, and 4-PRR layouts. The same dimensions and actuator

capabilities used for the non-redundant PPMs are employed for this analysis. For the 4-PRR, the prismatic joints' orientations are shown in Fig. 9c.

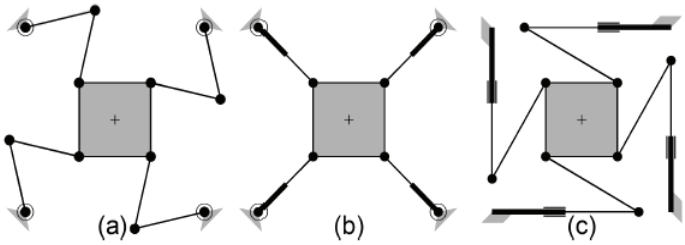

Fig. 9. Branch redundant PPM layouts: a) 4-RRR, b) 4-RPR, c) 4-PRR.

5.2 Wrench workspaces of planar parallel manipulators

In this work, the platform orientations are held constant at 0° and the assembly modes for the RRR and PRR architectures are shown in Figs. 7 to 9. Four analyses are considered:

a) Maximum force with a prescribed moment at $m_z = 0$, i.e., pure force analysis,
b) Maximum allowable force with an associated moment, i.e., absolute force analysis,
c) Maximum moment with a prescribed force at $f = 0$, i.e., pure moment analysis,
d) Maximum allowable moment with an associated Force, i.e., absolute moment analysis.

The third analysis ($f = 0$) is a special case that also involves the operational condition of prescribed isotropic and available forces. Examples of prescribed isotropic and available forces workspaces, where $f \neq 0$, can be found in Firmani et al. (2007b).

Figs. 10 to 18 show the wrench capabilities of the previously described manipulators. These capabilities are presented in two dimensional plots whose axes indicate the location of the mobile platform throughout the workspace [m]. At each location, either the maximum force or maximum moment capability is determined and illustrated with a dot using a grayscale gradient. Nonetheless, some of the magnitudes were very large compared to the rest of the results in the workspace. Large values are caused by the proximity of the manipulator to a singular configuration and this spoils the overall grayscale gradient.

Parallel manipulators are affected by inverse and direct singularities. An inverse singularity configuration usually occurs at the boundaries of the workspace. For the RRR architecture, a branch is either fully extended or folded back. For the RPR architecture, the displacement of a prismatic joint is zero. For the PRR architecture, the second link of a branch is perpendicular to the prismatic joint. Under these configurations, the manipulator cannot apply any force along one direction, but in theory it can sustain an infinite load. Similarly, the manipulator cannot apply any moment but in theory it can sustain an infinite moment, if an associated force goes to infinity. Since infinite wrench magnitudes would destroy the grayscale gradient, hence, the authors opted to cap these values.

A direct singularity occurs when the branch resultant forces together do not span an external wrench, i.e., the branch resultant forces intersect at a common point (planar pencil). If the branch forces intersect at infinity, an external force, normal to the branch forces, cannot be sustained, i.e., $f_{is} = 0$. If the intersection occurs somewhere else, an external moment applied to the mobile platform cannot be balanced by the actuators, i.e., $m_z = 0$.

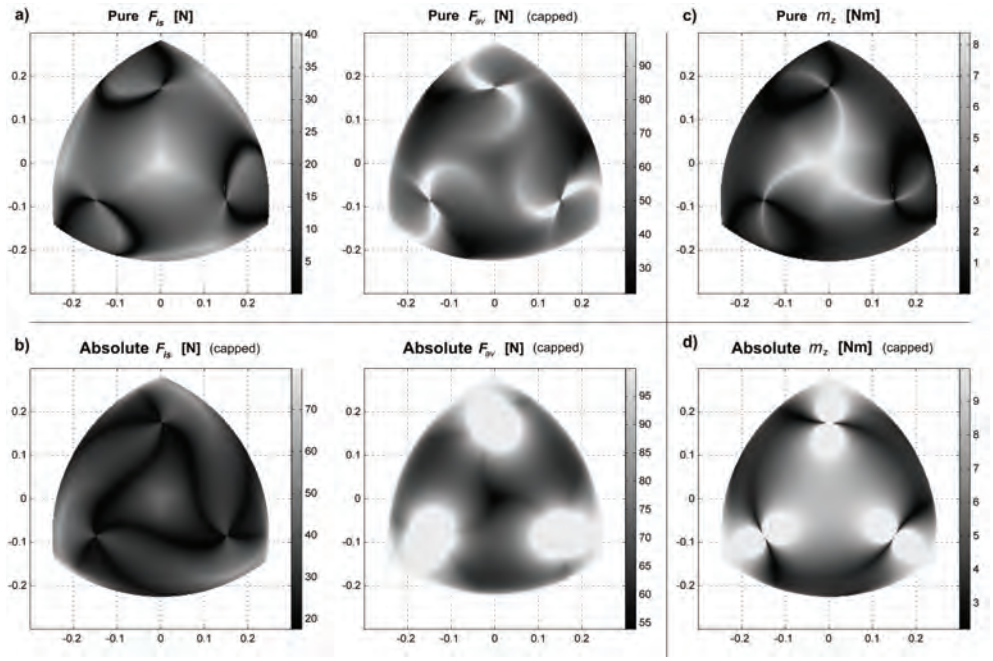

Fig. 10. Wrench workspaces for the 3-RRR PPM.

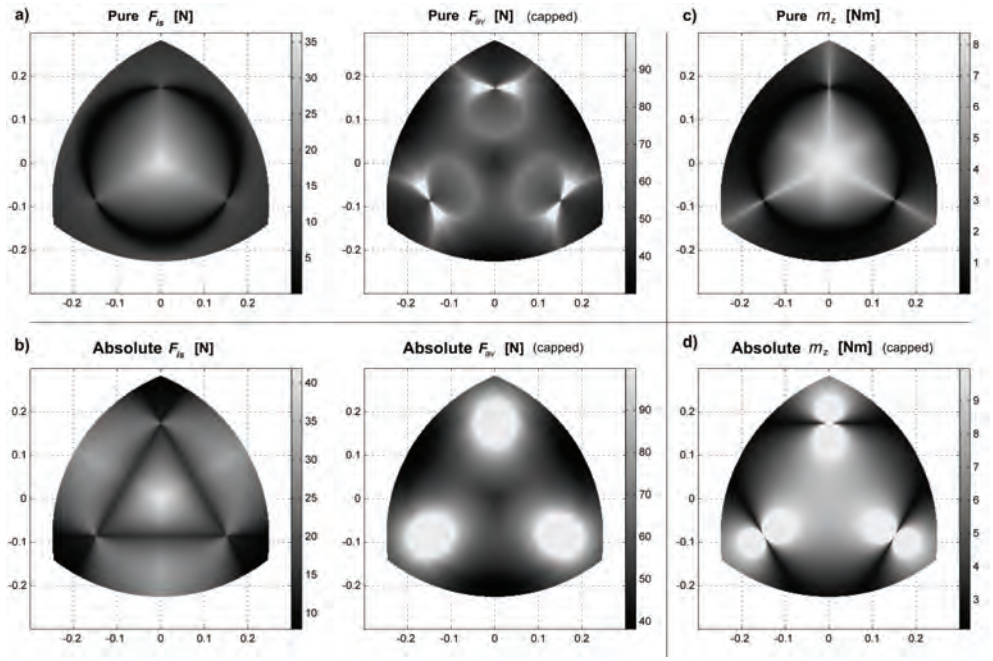

Fig. 11. Wrench workspaces for the 3-RPR PPM.

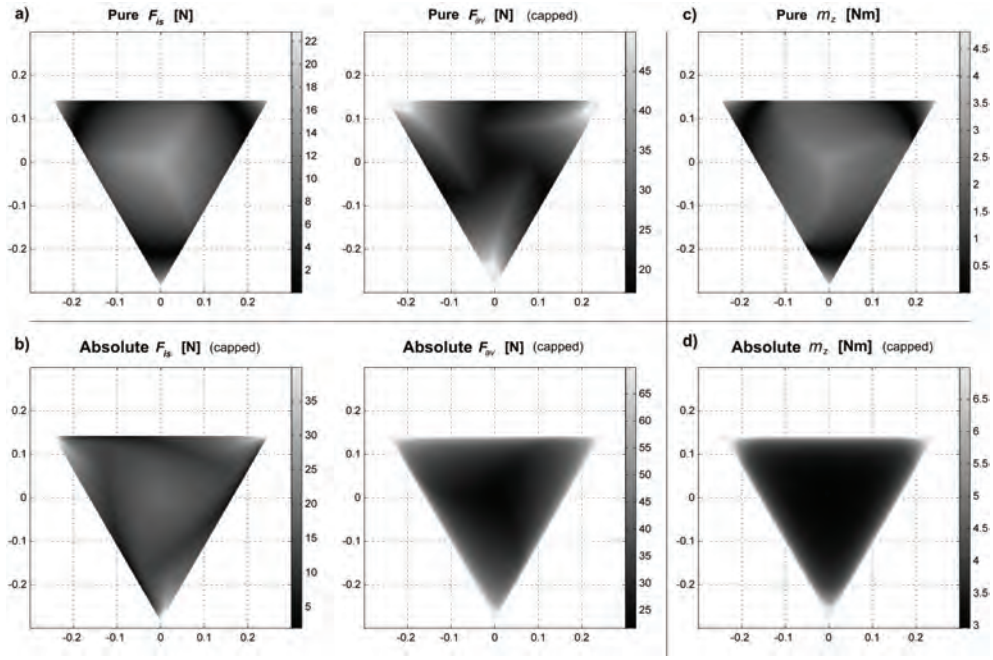

Fig. 12. Wrench workspaces for the 3-PRR PPM.

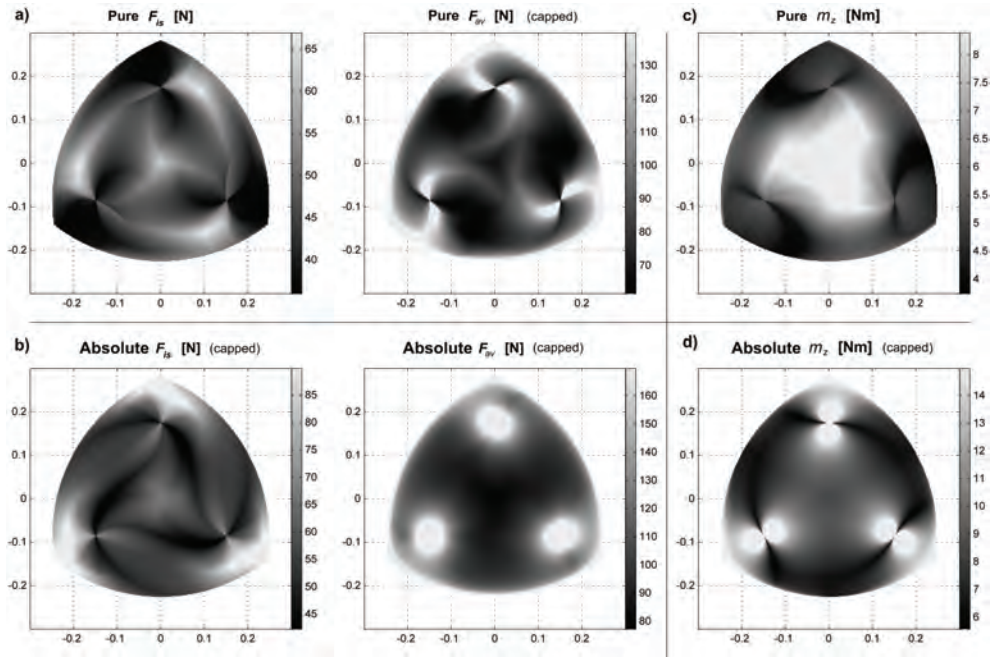

Fig. 13. Wrench workspaces for the 3-RRR PPM.

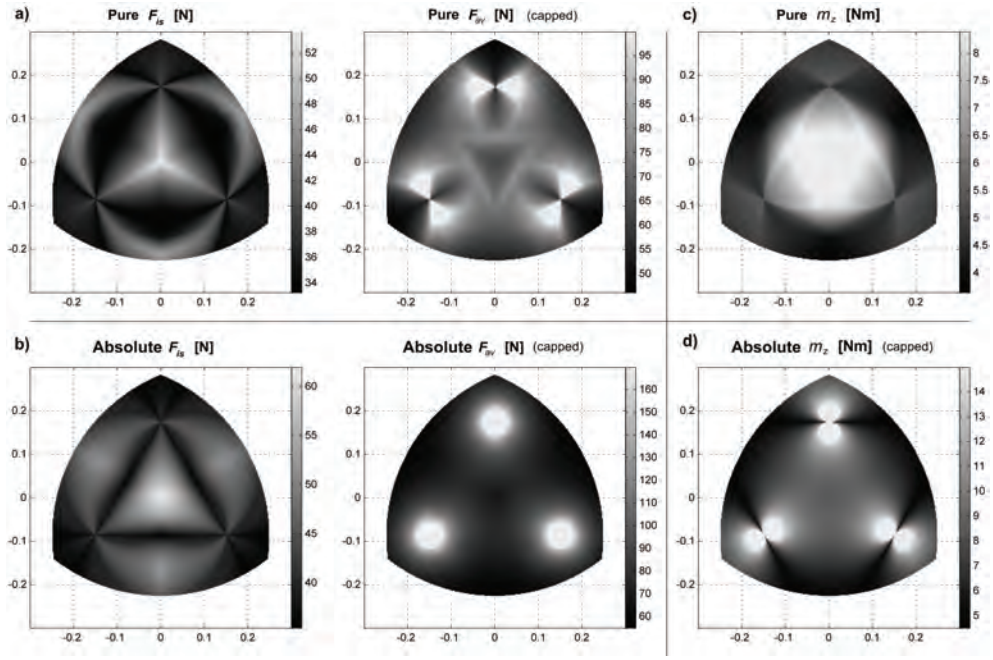

Fig. 14. Wrench workspaces for the 3-RPR PPM.

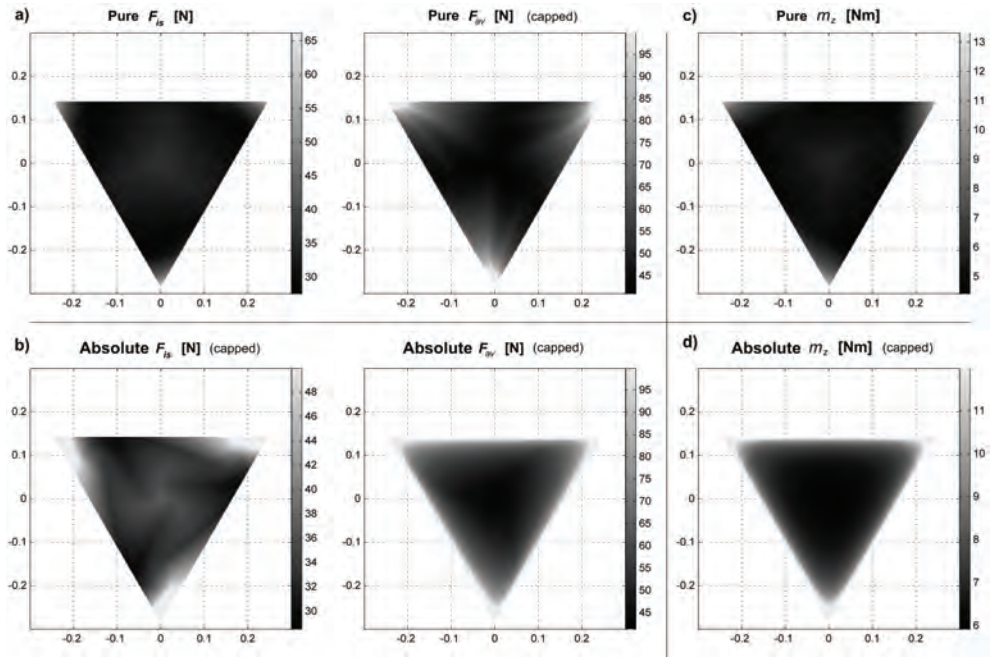

Fig. 15. Wrench workspaces for the 3-PRR PPM.

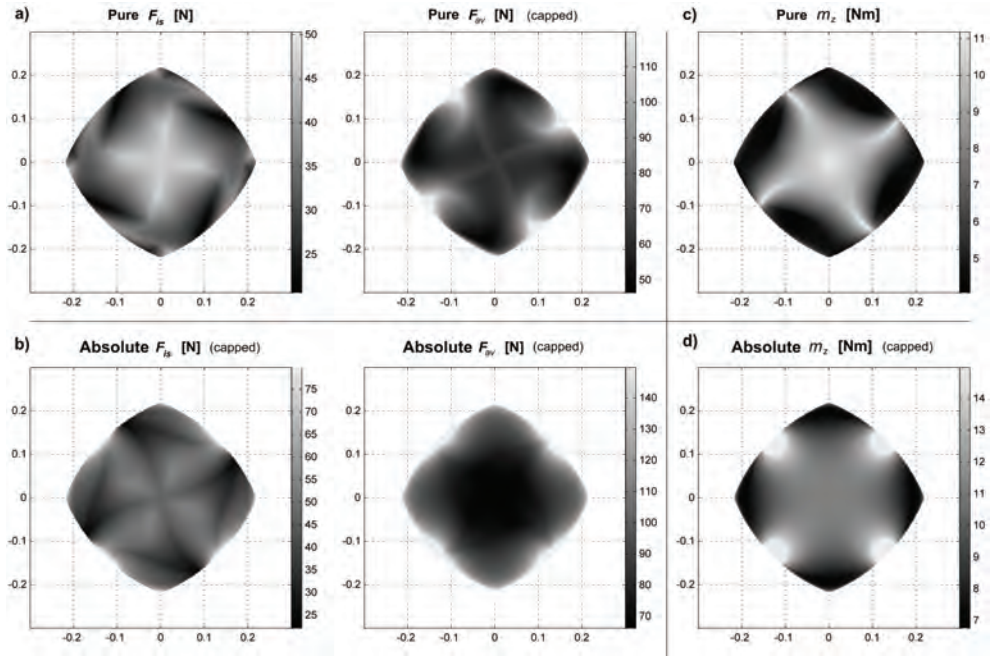

Fig. 16. Wrench workspaces for the 4-RRR PPM.

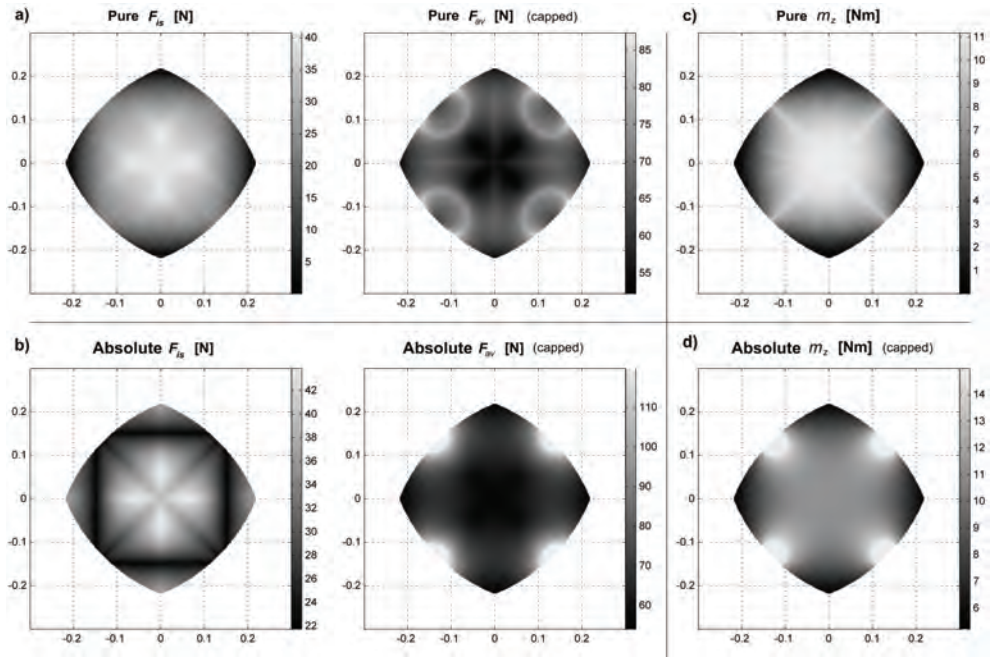

Fig. 17. Wrench workspaces for the 4-RPR PPM.

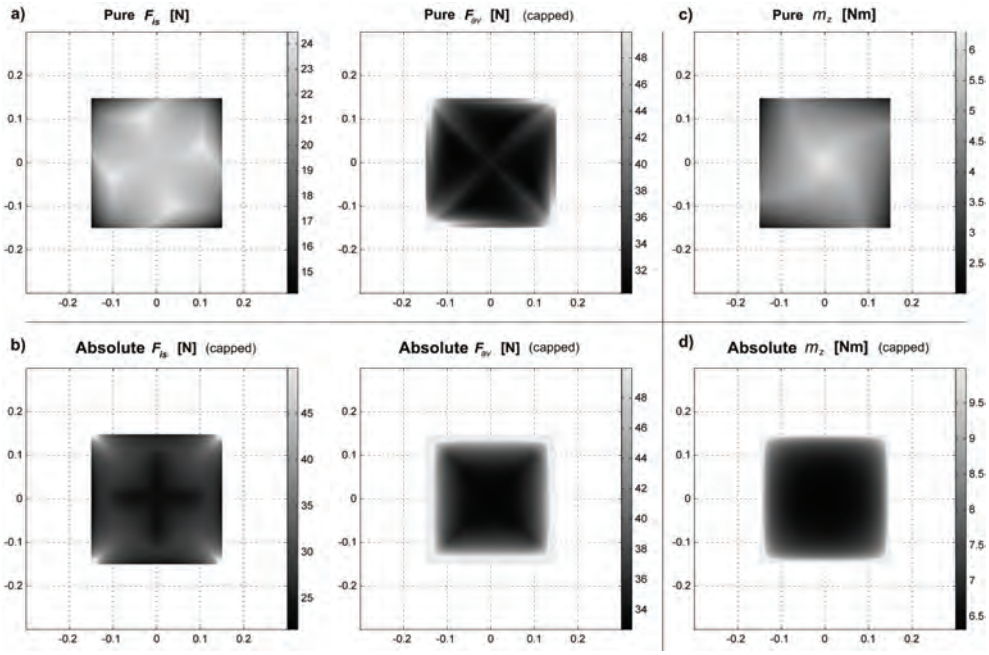

Fig. 18. Wrench workspaces for the 4-PRR PPM.

5.3 Discussion of the results

The plots show regions where larger forces or moments can be applied/sustained. Table 4 shows a numerical comparison of the different actuation layouts. Minimum and median values are adopted as indices of comparison and are denoted as min(∗) and $\tilde{*}$, respectively. These indices are preferred over maximum or mean values because they are not affected by infinite or very large results caused by singularities.

PPM Layout	Pure F_{is} [N]		Pure F_{av} [N]		Abs. F_{is} [N]		Abs. F_{av} [N]		Pure m_z [Nm]		Abs. m_z [Nm]	
	$\min(F_{is})$	$\tilde{F}_{is}$	$\min(F_{av})$	$\tilde{F}_{av}$	$\min(F_{is})$	$\tilde{F}_{is}$	$\min(F_{av})$	$\tilde{F}_{av}$	$\min(m_z)$	$\tilde{m}_z$	$\min(m_z)$	$\tilde{m}_z$
3-RRR	0.00	17.13	22.33	57.11	17.41	31.22	53.80	79.76	0.00	2.00	2.21	6.87
3-RPR	0.00	9.57	29.90	53.42	7.88	22.98	38.08	63.23	0.00	1.62	2.10	6.43
3-PRR	0.00	8.57	17.06	25.06	1.83	13.95	21.59	34.37	0.00	1.90	2.95	3.58
3-RRR	35.92	46.92	61.40	87.25	42.17	56.29	77.05	114.06	3.73	5.51	5.55	8.98
3-RPR	33.19	37.22	45.97	70.25	35.34	43.05	54.59	77.43	3.63	5.03	4.47	8.27
3-PRR	27.48	31.66	40.86	49.18	28.49	34.05	41.20	55.75	4.40	5.07	5.91	7.19
4-RRR	20.61	34.47	46.30	66.24	22.02	46.14	66.05	92.14	4.06	7.01	6.75	11.06
4-RPR	0.01	26.81	52.17	65.58	21.69	30.92	53.89	67.76	0.00	7.71	5.19	11.03
4-PRR	14.14	22.32	30.27	33.29	21.55	27.84	32.66	38.63	2.00	4.56	6.31	7.10

Table 4. Wrench performance indices of planar parallel manipulators.

The results clearly show that the addition of redundancy, whether in-branch or branch redundancy, has a dramatic improvement on the wrench capabilities for PPMs when compared to non-redundant PPMs. In particular, in-branch redundancy provides greater forces; whereas, branch redundancy offers greater moments.

6. Future research

A number of possible avenues for future investigation exist. For this work, the orientation of the platform was kept constant. Investigating the effects on wrench capabilities for PPMs by varying the orientation of the platform would provide a better understanding of the full range of wrench capabilities of a given architecture. Another avenue of investigation would be determining the effects that modifying the geometric parameters of a PPM architecture has on its wrench capabilities. Also, exploring the effects on the wrench capabilities of changing the assembly modes for a given architecture could be conducted. Application of the proposed indices to spatial PMs would be a further area to explore.

7. Conclusions

This work presents a method to understand and quantify wrench capabilities of PPMs. Wrench capabilities are determined by projecting the actuator torque capabilities into the wrench space. This projection is a linear transformation that leads to a convex set, i.e., a wrench polytope. To numerically evaluate wrench polytopes, six wrench performance indices are derived. Each index is associated to a particular operational condition of the manipulator. These indices are plotted throughout the workspace of the manipulator. As a design tool, the wrench workspaces allow for easy visualization of the differences in wrench capabilities between different PPM architectures. For an existing manipulator, this visual representation can be employed to improve path planning.

The wrench capability analysis is implemented to three non-redundant layouts: 3-RRR, 3-RPR, and 3-PRR. In addition, the effects of including in-branch redundancy (3-RRR, 3-RPR, and 3-PRR) and branch redundancy (4-RRR, 4-RPR, and 4-PRR) are presented. It is concluded that in-branch redundancy yields greater forces; whereas, branch redundancy offers greater moments.

8. References

Bicchi, A., Melchiorri, C., & Balluchi, D. (1995) On the Mobility and Manipulability of General Multiple Limb Robotic Systems, *IEEE Transactions on Robotics and Automation,* Vol. 11, No. 2, (Apr. 1995), pp. 215-228.

Buttolo, P. & Hannaford, B. (1995) Advantages of Actuation Redundancy for the Design of Haptic Displays, *Proceedings of the 1995 ASME International Mechanical Engineering Congress and Exposition – Part 2,* pp. 623-630, San Francisco, CA, USA, Nov. 1995.

Chand, D. R. & Kapur, S. S. (1970) An Algorithm for Convex Polytopes, *Journal of the Association for Computing Machinery*, Vol. 17, No. 1, (Jan. 1970), pp. 78-86.

Chiacchio, P., Bouffard-Vercelli, Y., & Pierrot, F. (1996) Evaluation of Force Capabilities for Redundant Manipulators, *Proceedings of the 1996 IEEE International Conference on Robotics and Automation*, Vol. 4, pp. 3520-3525, Minneeapolis, MN, USA, Apr. 1996.

Chiacchio, P., Bouffard-Vercelli, Y., & Pierrot, F. (1997) Force polytope and force ellipsoid for redundant manipulators, *Journal of Robotic Systems*, Vol. 14, No. 8, Aug. 1997, pp. 613-620.

Ebrahimi, I., Carretero, J. A., & Boudreau, R. (2007) 3-PRRR Redundant Planar Parallel Manipulator: Inverse Displacement, Workspace and Singularity Analyses, *Mechanism and Machine Theory*, Vol. 42, No. 8, (Aug. 2007), pp. 1007-1016.

Finotello, R., Grasso, T., Rossi, G., & Terribile, A. (1998) Computation of Kinetostatic Performances of Robot Manipulators with Polytopes, *Proceedings of the 1998 IEEE International Conference on Robotics and Automation*, Vol. 4, pp. 3241-3246, Leuven, Belgium, May 1998.

Firmani, F. & Podhorodeski, R. P. (2004) Force-Unconstrained Poses for a Redundantly-Actuated Planar Parallel Manipulator, *Mechanism and Machine Theory*, Vol. 39, No. 5, (May 2004), pp. 459-476.

Firmani, F. & Podhorodeski, R. P. (2005), Force-Unconstrained Poses for Parallel Manipulators with Redundant Actuated Branches, *Transactions of the CSME*, Vol. 29, No. 3, (Sept. 2005), pp. 343-356.

Firmani, F., Zibil, A., Nokleby, S. B., & Podhorodeski, R. P. (2007a) Wrench Capabilities of Planar Parallel Manipulators- Part I: Wrench Polytopes and Performance Indices, *accepted for publication in Robotica*.

Firmani, F., Zibil, A., Nokleby, S. B., & Podhorodeski, R. P. (2007b) Wrench Capabilities of Planar Parallel Manipulators- Part II: Redundancy and Wrench Workspace Analysis, *accepted for publication in Robotica*.

Gallina, P. Rosati, G., & Rossi, A. (2001) 3-d.o.f. Wire Driven Planar Haptic Interface, *Journal of Intelligent and Robotic Systems*, Vol. 32, No. 1, (Sept. 2001), pp. 23 - 36.

Garg, V., Carretero, J. A., & Nokleby, S. B. (2007) Determining the Force and Moment Workspace Volumes of Redundantly-Actuated Spatial Parallel Manipulators, *Proceedings of the 2007 ASME Design Engineering Technical Conference, ASME*, Las Vegas, NV, USA, Sept. 2007.

Hwang, Y. S., Lee, J., & Hsia, T. C. (2000) A Recursive Dimension-Growing Method for Computing Robotic Manipulability Polytope, *Proceedings of the 2000 IEEE International Conference on Robotics and Automation*, Vol. 3, pp. 2569-2574, San Francisco, CA, USA, Apr. 2000.

Kokkinis, T. & Paden, B. (1989). Kinetostatic Performance Limits of Cooperating Robot Manipulators Using Force-Velocity Polytopes, *Proceedings of the ASME Winter Annual Meeting,* pp. 151-155, San Francisco, CA, USA, Dec. 1989.

Krut, S., Company, O., & Pierrot, F. (2004a) Velocity Performance Indices for Parallel Mechanisms with Actuation Redundancy, *Robotica*, Vol. 22, No. 2, (Mar. 2004), pp. 129-139.

Krut, S., Company, O., & Pierrot, F. (2004b) Force Performance Indexes for Parallel Mechanisms with Actuation Redundancy, Especially for Parallel Wire-Driven Manipulators, *Proceedings of 2004 IEEE/RSJ International Conference on Intelligent Robots and Systems*, Vol. 4, pp. 3936-3941, Sendai, Japan, Sept.-Oct. 2004.

Kumar, V. & Waldron, K. J. (1988) "Force Distribution in Closed Kinematic Chains," *Proceedings of the 1988 IEEE International Conference on Robotics and Automation*, pp. 114-119, Philadelphia, PA, USA, Apr. 1988.

Lee, S. & Kim, S. (1991) A Self-Reconfigurable Dual-Arm System, *Proceedings of the1991 IEEE International Conference on Robotics and Automation*, Vol. 1, pp. 164-169, Sacramento, CA, USA, Apr. 1991.

Lee S. & Kim, S. (1993) Kinematic Analysis of Generalized Parallel Manipulator Systems, *Proceedings of the 32nd IEEE Conference on Decision and Control*, Vol. 2, pp. 1097-1102, San Antonio, TX, USA, Dec. 1993.

Lee, J. (1997) A Study on the Manipulability Measures for Robot Manipulators, *Proceedings of 1997 IEEE/RSJ International Conference on Intelligent Robots and Systems*, Vol. 3, pp. 1458-1465, Grenoble, France, Sept. 1997.

Lee, J. & Shim, H. (2004) On the Dynamic Manipulability of Cooperating Multiple Arm Robot Systems, *Proceedings of 2004 IEEE/RSJ International Conference on Intelligent Robots and Systems*, Vol. 2, pp. 2087 - 2092, Sendai, Japan, Sept.-Oct. 2004.

Merlet, J. P. (1996) Redundant Parallel Manipulators, *Journal of Laboratory Robotics and Automation*, Vol. 8, No. 1, (Feb. 1996)., pp. 17-24

Nahon, M. A. & Angeles, J. (1992) Real-Time Force Optimization in Parallel Kinematic Chains Under Inequality Constraints, *IEEE Transactions on Robotics and Automation*, Vol. 8, No. 4, (Aug. 1992), pp. 439-450.

Nokleby, S. B., Fisher, R., Podhorodeski, R. P., & Firmani, F. (2005). Force Capabilities of Redundantly-Actuated Parallel Manipulators, *Mechanism and Machine Theory*, Vol. 40, No. 5, (May 2005), pp. 578-599.

Nokleby, S. B., Firmani, F., Zibil, A., & Podhorodeski, R. P. (2007a) Force-Moment Capabilities of Redundantly-Actuated Planar-Parallel Architectures, *Proceedings of the IFToMM 2007 World Congress*, 6 pages, Besançon, France, June 2007.

Nokleby, S. B., Firmani, F., Zibil, A., & Podhorodeski, R. P. (2007b) An Analysis of the Force-Moment Capabilities of Branch-Redundant Planar-Parallel Manipulators, *Proceedings of the 2007 ASME Design Engineering Technical Conference, ASME*,), 8 pages, Las Vegas, NV, USA, Sept. 2007.

Rockafellar, R. T. (1997, first printed 1970). *Convex Analysis*, Princeton University Press, Princeton, NJ, USA.

Tao, J.M. & Luh, J. Y. S. (1989) Coordination of Two Redundant Manipulators, *Proceedings of the 1989 IEEE International Conference on Robotics and Automation*, pp. 425-430, Scottsdale, AZ, USA, May 1989.

Visvanathan, V. & Milor, L. S. (1986) An Efficient Algorithm to Determine the Image of a Parallelepiped Under a Linear Transformation, *Proceedings of 2nd Annual Symposium on Computational Geometry*, pp. 207-215, Yorktown Heights, NY, USA, June 1986.

Wang, J., & Gosselin, C. M. (2004) Kinematic Analysis and Design of Kinematically Redundant Parallel Mechanisms, *Transactions of the ASME, Journal of Mechanical Design*, Vol. 126, No. 1, (Jan. 2004), pp. 109-118.

Yoshikawa, T. (1985) Manipulability of Robotic Mechanisms, *International Journal of Robotics Research,* Vol. 4, No. 2, (Mar. 1985), pp. 3-9.

Yoshikawa, T. (1990). *Foundations of Robotics: Analysis and Control,* The MIT Press, Cambridge, MA, USA.

Zibil, A., Firmani, F., Nokleby, S. B., & Podhorodeski, R. P. (2007) An Explicit Method for Determining the Force-Moment Capabilities of Redundantly-Actuated Planar Parallel Manipulators, *Transactions of the ASME, Journal of Mechanical Design*, Vol. 129, No. 10, (Oct. 2007), pp. 1046-1055.